THE WAVELENGTH OF OSCILLATION SAND RIPPLES

Kaneko, Arata
Research Institute for Applied Mechanics, Kyushu University : Research Associate

https://doi.org/10.5109/6776439

出版情報：Reports of Research Institute for Applied Mechanics. 28 (88), pp.57-71, 1980-09. 九州大学応用力学研究所

Reports of Research Institute for Applied Mechanics
Vol. XXVIII. No. 88, 1980

THE WAVELENGTH OF OSCILLATION SAND RIPPLES

By Arata KANEKO *

The wavelengh of sand ripples formed under oscillatory flow and water waves, i. e. oscillation sand ripples has been well understood by correlating with the representative length-scales of a flow and a bed material; the stroke (twice the amplitude) of fluid oscillation d_0, the thickness of the Stokes layer δ and the median diameter of sand particles D.
Some empirical formulae are presented which fit the result of experiments and field observations.

Key words: Sand ripples, Oscillatory flow, Wavelength

1. Introduction

The oscillation sand ripples have been observed by many workers [1]~[10] in both laboratory tanks and nearshore zones. These observations made it possible to predict roughly the formation region and the geometrical properties of the ripples. However, the data of the wavelength of the ripples scatter considerably in the previous analyses and the detailed investigation seems to be necessary for obtaining a better understanding of the wavelength.

It was reported by Kaneko & Honji [11] that in highly viscous fluids ripples are made up inducing steady streaming, and by Honji et al. [12] that with the decrease of viscosity the types of flows over ripples are changed from steady streaming to separation vortices.
Kaneko [13] also showed that the wavelength of ripples in highly viscous fluids depends on δ $(=\sqrt{2\nu/\omega})$ rather than d_0, the quantities ν and ω being respectively the kinematic viscosity of a fluid and the angular frequency of fluid oscillation. The main purpose of this study is to obtain an unified concept on the wavelength of ripples by clarifying the influence of D in addition to d_0 and δ. The growth of the wavelength accompanied by the development of ripples is also discussed in parallel with the variation of flows over ripples.

* Research Associate, Research Institute for Applied Mechanics, Kyushu University

2. Experiments

Experiments were carried out in a closed-type tunnel, as sketched in Fig. 1. The horizontal test section of the tunnel was 180 *cm* in length, and 25 *cm* in width and in height. Water in the tunnel was oscillated by a

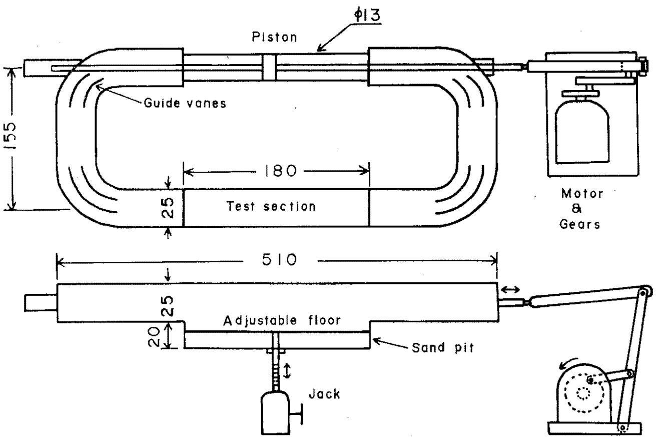

Fig. 1. Schematic diagrams (plan and side views) of the experimental tunnel (dimension in cm).

motor-driven piston. The test section was equipped with a sand pit, which was used to set up a sand bed, i. e. a thick layer of test particles. Flow in the test section was made uniform by guide vanes put in every corner of the tunnel. Experiments using glycerine-water solutions with various values of ν were made in a U-tube, of which the rectangular cross section was 12*cm* × 12*cm*. Details of the tube are shown in the preceding paper [11]. The value of ν was varied up to 2.08 cm^2/s. The maximum values of d_0 and f ($=\omega/2\pi$) for each apparatus are presented in Table 1. Spherical glass beads of density (ρ_s) 2.43 g/cm^3 and median diameter (D) 0.007 ~ 0.086 *cm* were used as test particles. The waveheight of ripples was measured by means of a

Table 1 The maximum values of do and f of the apparatus

	Closed-type tunnel	U-tube
$(d_0)_{max}$	70 *cm*	14 *cm*
$(f)_{max}$	1.3 Hz	2.6 Hz

ultrasonic bottom profiler, of which the resolution was up to 1 mm. Photographs were taken through the transparent side walls of the tunnel and the tube at various stages of ripple development using a 35 mm camera.

3. Dimensional Analysis

The wavelength (L) of oscillation sand ripples may be correlated with other quantities by the following relation

$$L = \psi\ (d_0,\ H,\ \omega,\ \nu,\ \rho_f,\ D,\ \rho_S,\ g\ ), \qquad (1)$$

where H, ρ_f and g are the waveheight of ripples, the density of a fluid and the acceleration due to gravity. Symbol ψ stands for a function. Based on dimensional analysis, we obtain a relation among six nondimensional parameters

$$\frac{L}{d_0} = F\left(\frac{d_0}{\delta},\ \frac{H}{\delta},\ \frac{u_m}{\sqrt{(\rho_S/\rho_f - 1)\,gD}},\ \frac{D}{\delta},\ \frac{\rho_S}{\rho_f}\right), \qquad (2)$$

in which $u_m = d_0\ \omega/2$. The relation including explicitly the steepness (H/L) is given by rewritting eq. 2 as

$$\frac{H}{L} = F'\left(\frac{d_0}{\delta},\ \frac{H}{\delta},\ \frac{u_m}{\sqrt{(\rho_S/\rho_f - 1)\,gD}},\ \frac{D}{\delta},\ \frac{\rho_S}{\rho_f}\right), \qquad (2)'$$

where symbols F and F′ stand for functions. It should be remarked that the H dependence of L is considered which has been neglected in the analyses of other wokers [3) 7) 14)]. In ep. 2, the nondimensional parameters L/d_0, d_0/δ and H/δ coincide with those appearing in the analysis of oscillatory flow over a rigid wavy wall and the remaining parameters $u_m/\sqrt{(\rho_S/\rho_f - 1)\,gD}$, D/δ and ρ_S/ρ_f relate to the mobility of a bed material. Since only particles with a density nearly equal to that of quartz sands (= 2.65 g/cm³) are used in the present analysis, the value of ρ_S/ρ_f is considered as a constant. Therefore, we retain ρ_S/ρ_f only in the third term of the right-hand side of eps. 2 and 2′.

The oscillation sand ripples are classified on a ($u_m/\sqrt{(\rho_S/\rho_f - 1)\,gD}$, D/δ) plane showing the mobility of a bed material. Figure 2 shows such a classification based on the stationary form of ripples.

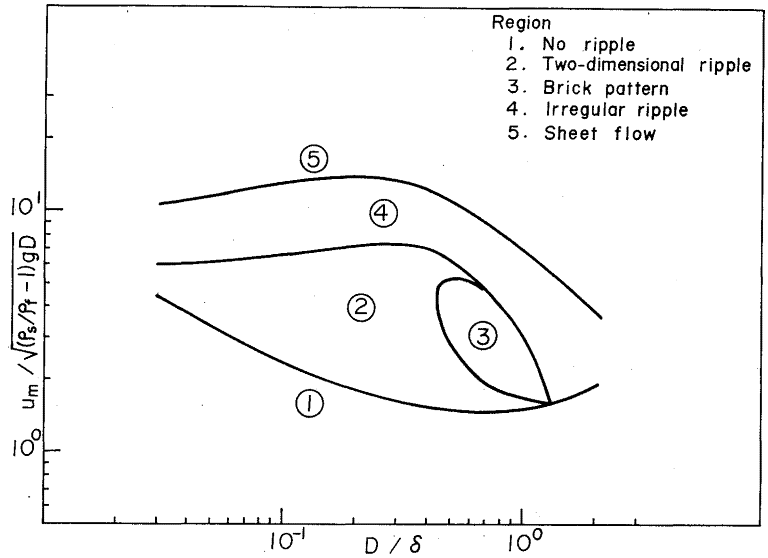

Fig. 2. Classification of ripples.

In Region 1, the ripples could not form although a few of particles on the bed surface were in motin. In Region 5, the ripple also disappeared beacuse of strong oscillation of beds called the sheet flow. The ripples with two-dimensional forms were observed in Region 2, and the brick pattern of Bagnold [1] in Region 3. Region 4 is the transition region from rippled beds to sheet flow and the ripple forms are irregular.

The critical lines for ripple initiation, transition bed and sheet flow agree roughly with those of Komar & Miller [15] and Dingler & Inman[7].

The ripples of Regions 2 and 3 develop slowly as the result of consecutive piling-up of sand particles along the bed surface, and almost maintain their original shapes even after fluid oscillation has been stopped.

The wavelength of such ripples may be given by the simple relation

$$\frac{L}{d_0} = f\left(\frac{d_0}{\delta}, \frac{H}{\delta}\right), \qquad (3)$$

independently of the characteristic properties of a bed material.

Symbol f stands for a function, and parameters d_0/δ and H/δ are the square root of the Reynolds number for oscillatory flow over a flat wall and the relative roughness of ripples, respectively. The validity of eq. 3 will be discussed later by comparing with the data of real ripples.

4. Development of Ripples

The observed values of L/d_0 at three stages of ripple develoment, i. e. the initial stage, the onset of separation vortices and the stationary stage are plotted against d_0/δ in Fig. 3. At $d_0/\delta < 12$, the initial wavelength is nearly equal to that of stationary ripples.
Kaneko[13] predicted the dominant wavelength of ripples in this region by estimating numerically the wall shear stress due to steady streaming and obtained the relation

$$\frac{L}{d_0} = 50.6 \left(\frac{d_0}{\delta}\right)^{-1.48}, \qquad (4)$$

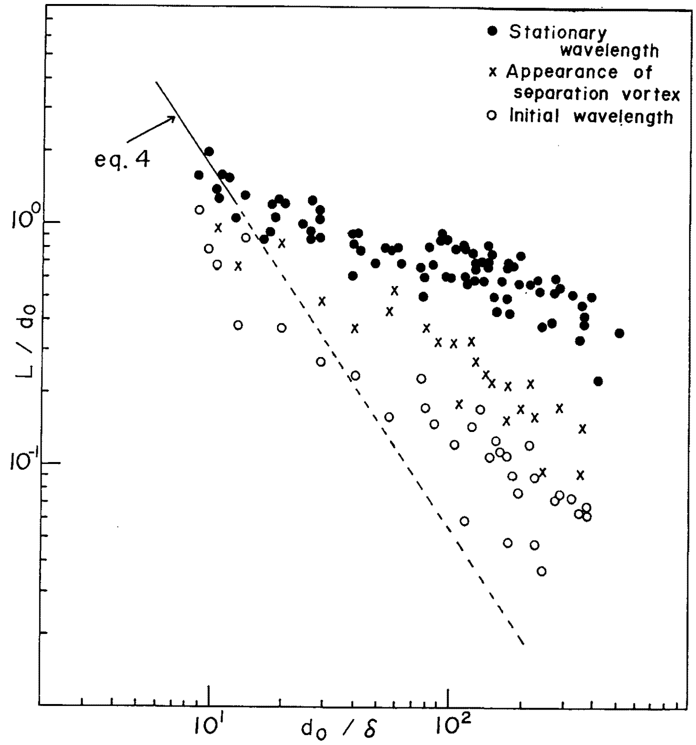

Fig. 3. Growth of the wavelength of ripples.

which is in good agreement with the plotted data at $d_0 / \delta < 12$. Figure 4 shows the development process of ripples observed at $d_0 / \delta = 10.7$. After fluid oscillation started, gentle rises began to cover the bed surface (Fig. 4a) and subsequently grew into the crests of regular ripples (Fig. 4b). The ripples reached a stationary state keeping the wavelength nealy constant (Figs. 4c and d). Throughout all the stages of development, ripple crests were rounded and no flow separation was seen.

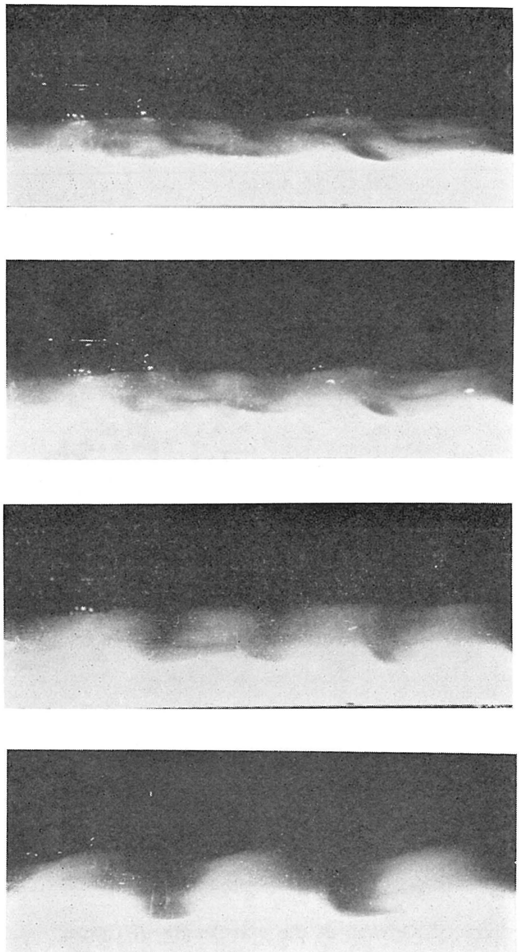

(a)

(b)

(c)

(d)

Fig. 4. Development of ripples at $d_0 / \delta = 10.7$; $d_0 = 8.9$ cm, $f = 0.96$ Hz, $\nu = 2.08$ cm^2 / s, $D = 0.034$ cm, $L_S = 11.3$ cm, and $H_S = 1.2$ cm.

(a) t = 156 sec (b) t = 269 sec

(c) t = 379 sec (d) t = 2100sec

It is seen from Fig. 3 that the difference between the wavelengths at initial and stationary stages increases with d_0 / δ. Figure 5 shows the development process of ripples observed at $d_0 / \delta = 354$. The development process started with the appearance of long and narrow crests (Fig. 5a) similar to the particle wave of Kaneko & Honji [16]. Although the crest pattern was considerably irregular, the wavelength of ripples measured in the direction of fluid oscillation was roughly constant.

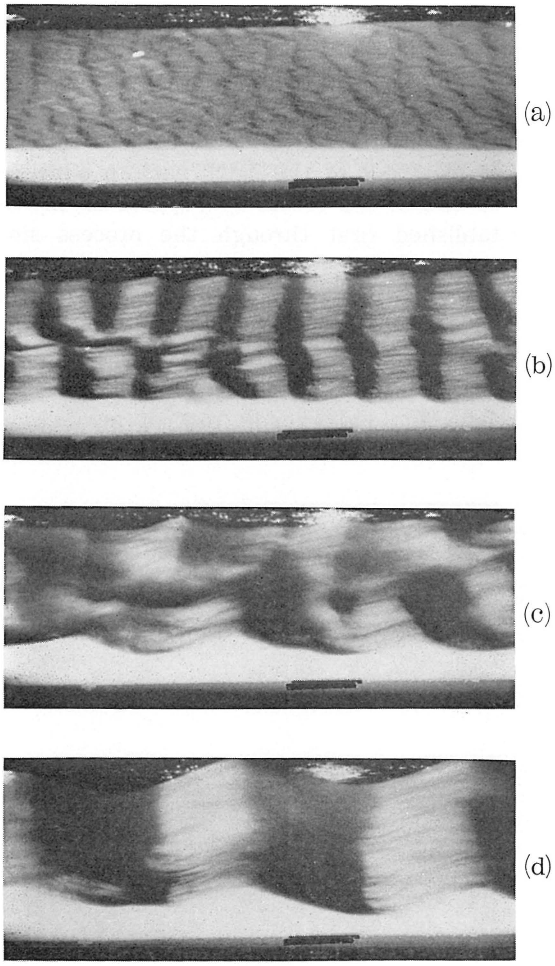

Fig. 5. Development of ripples at $d_0 / \delta = 354$ (Scale bar : 5 cm) ;
$d = 40.7$ cm, $f = 0.24$ Hz, $\nu = 0.010$ cm^2 / s,
$D = 0.028$ cm, $L_S = 15.8$ cm, and $H_S = 2.2$ cm.
(a) $t = 70$ sec (b) $t = 210$ sec
(c) $t = 634$ sec (d) $t = 1506$ sec

The average value of the wavelength was much smaller than d_0. No flow separation over the ripples took place at this stage. The wavelength continued to increase slowly in parallel with the growth of the waveheight. When the waveheight reached at a critical value, flows over the ripples began to separate from the crests. The ripples became remarkably regular immediately after flow separation developed fully (Fig. 5b), and reached a stationary state repeating the variation of their forms (Figs. 5c and d). At large d_0/δ, the data of the initial wavelength scatter near a broken line drawn by extrapolating eq. 4 to the region of $d_0/\delta > 12$. The initial stage of the ripples seems to be dominated by steady streaming. The data also show that separation vortices begin to occur when H/δ exceeds about 3.0.

The brick pattern was observed to form at $50 < d_0/\delta < 200$. Figure 6 shows the typical development of the brick pattern observed at $d_0/\delta = 114$. As shown in Figs. 6a and b, the crests epui-spaced in the direction of fluid oscillation were established first through the process similar to that of Fig. 5. Then, the crests running along the direction of fluid oscillation began to form and the resulting crest pattern became oblique (Fig. 6c). Figure 6d shows the clear oblique pattern photographed after fluid oscillation has been stopped. The formation of such ripples may be related to the brick pattern streaming induced in oscillatory flow around a circular cylinder (Honji[17]) and over a row of semi-circular cylinders on a flat wall (Matsunaga & Honji[18]).

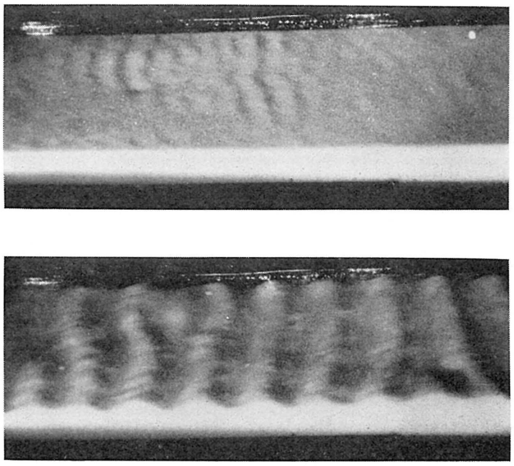

(a)

(b)

Fig. 6. Development of brick patterns at $d_0/\delta = 114$
Scale bar: 5 cm); $d_0 = 6.0$ cm, $f = 1.2$ Hz, $\nu = 0.011 cm^2/s$, $D = 0.028$ cm, $L_1 = 5.0$ cm, $L_2 = 11.0$cm, and $H_S = 0.8$ cm.
(a) $t = 9$ sec (b) $t = 97$ sec
(c) $t = 165$ sec (d) $t = 285$ sec

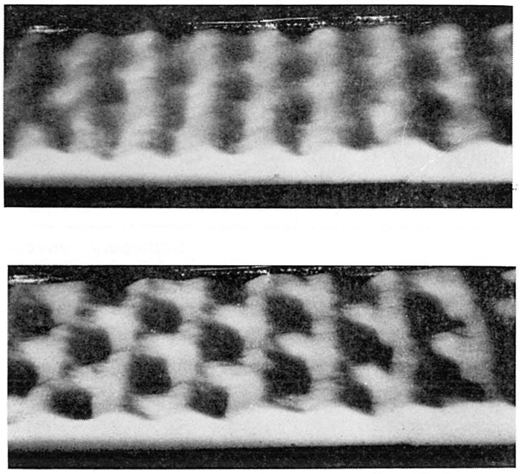

(c)

(d)

5. Wavelength of Stationary Ripples

The wavelength of stationary ripples observed in oscillatory-flow tunnels (Author and Carstens et al. [6]) and wave tanks (Kennedy & Falcon [4] and Miller & Komar [9]) is plotted in Fig. 7 by using the same co-ordinates as those of Fig. 3.

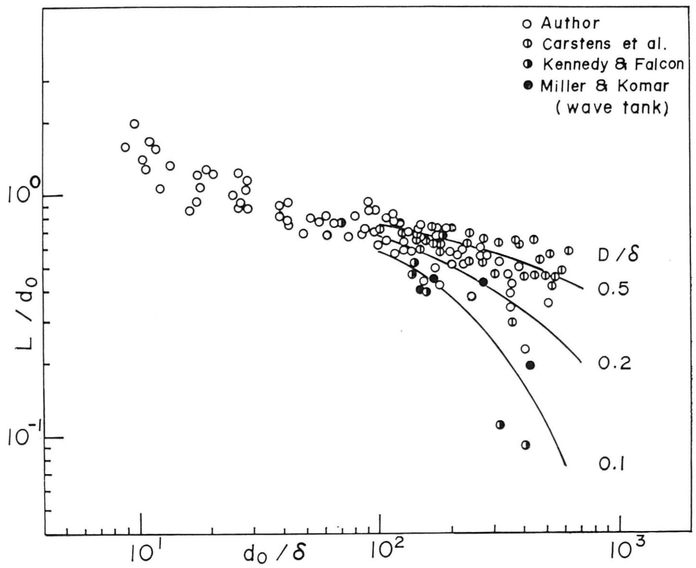

Fig. 7, Wavelength of stationary ripples plotted against d_0 / δ (Experimental results) .

The plotted data become to depend remarkably on D/δ at $d_0/\delta > 100$. The amount of sand particles suspended from rippled beds into flow are influenced by D/δ and the rapid enhancement of these particles seems to inhibit the furthur growth of the waveheight of ripples.

The data collapsing on the region of $d_0/\delta > 100$ of Fig. 7 are again plotted in Fig. 8 using d_0/D instead of d_0/δ as a horizontal axis. The data at $d_0/D < 1{,}000$ are well approximated by the relation

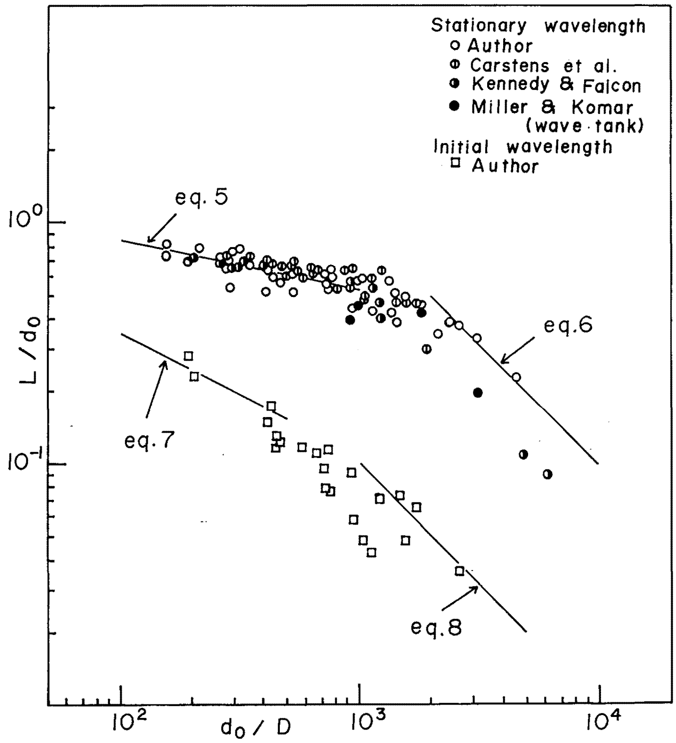

Fig. 8. Wavelength of stationary ripples plotted against d_0/D (Experimental results).

$$\frac{L_S}{d_0} = 2.1\left(\frac{d_0}{D}\right)^{-1/5}, \qquad (5)$$

where L_S is the wavelength in a stationary state. With increasing d_0/D, the data approach to the relation

$$L_S = 1{,}000\ D, \qquad (6)$$

given by Yalin [19] for the ripples formed under an unidirectional flow. The observed values of the initial wavelength (L_i) are also plotted in Fig. 8. At $d_0/D < 1{,}000$, the data agree roughly with the relation

$$\frac{L_P}{d_0} = 3.5 \left(\frac{d_0}{D} \right)^{-1/2}, \qquad (7)$$

given by Kaneko & Honji [16] for the wavelength (L_P) of the particle wave. With increasing d_0 / D, the data also approach to the relation

$$L_i = 100 \text{ D}. \qquad (8)$$

which is independent of d_0.

The field data of Inman[2] and Miller & Komar[10] for L_S are plotted in Fig. 9. The result of the field observation gives the value of L_S larger than the experimental value. This seems to be caused by the accurancy of the field observation and the insufficient development of the ripples. It should be noted that most of the field data scatter in the neighbourhood of a line for eq. 6.

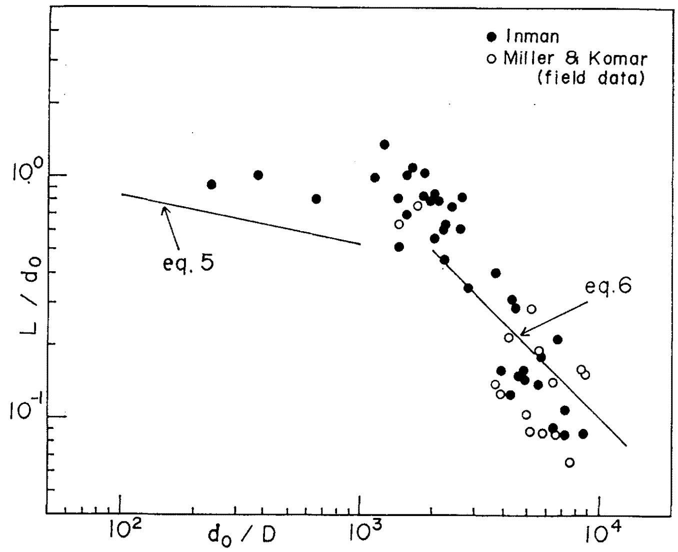

Fig. 9. Wavelength of ripples observed on a sea floor.

The steepness (H_S / L_S) of stationary ripples observed at $d_0 / \delta > 100$ by several workers is plotted against d_0 / D in Fig. 10. The data at $d_0 / D < 1{,}000$ are approximated by the relation

$$\frac{H_S}{L_S} = 0.15, \qquad (9)$$

and the value of H_S / L_S decreases gradually with increasing d_0 / D.

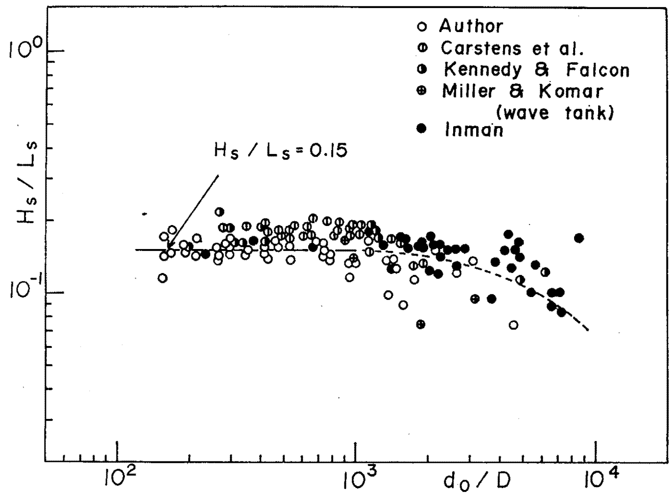

Fig. 10. Steepness of stationary ripples.

Table 2 The raw data of the brick pattern

		D (cm)	d_O (cm)	f (Hz)	ν (cm^2/s)	L_1 (cm)	L_2 (cm)	H_S (cm)
Closed-type tunnel	Exp. 1	0.047	12.6	0.85	0.011	9.1	18.2	1.4
	2	0.047	12.6	0.71	0.011	9.2	17.0	1.3
	3	0.047	7.5	1.09	0.011	5.3	8.5	0.9
	4	0.047	7.5	0.94	0.011	5.7	7.0	0.8
	5	0.028	10.0	1.01	0.010	6.7	10.6	1.0
	6	0.028	10.0	0.97	0.010	7.0	9.9	1.0
	7	0.028	8.1	1.09	0.011	5.7	7.2	0.9
	8	0.028	8.1	1.14	0.011	6.2	10.7	0.9
	9	0.028	6.0	1.33	0.011	5.0	11.0	0.8
	10	0.028	6.0	1.11	0.011	4.9	9.2	0.7
	11	0.028	4.7	1.33	0.010	4.1	7.5	0.6
	12	0.028	4.7	1.25	0.010	4.4	9.1	0.8
	13	0.028	4.7	1.21	0.010	4.1	7.7	0.6
U-tube	Exp.14	0.047	3.0	1.70	0.012	2.4	4.9	0.6
	15	0.047	3.0	1.26	0.012	2.4	7.4	—
	16	0.028	4.9	1.62	0.010	3.1	5.4	0.4
	17	0.020	3.1	1.97	0.009	2.3	4.5	0.4
	18	0.020	2.7	2.22	0.010	2.0	3.4	0.4

The wavelength of the brick pattern in a stationary state are here discussed briefly. The raw data of the brick pattern observed in the present experiment are presented in Table 2. L_1 and L_2 are respectively the wavelengths of ripples equi-spaced in two directions parallel to fluid oscillation and normal to it. The observed values of L_1 and L_2 are plotted against do in Fig. 11, and the plotted data fit the following relations

$$L_1 = 0.7\ d_0, \qquad (10)$$

$$1.0\ L_1 < L_2 < 3.0\ L_1$$

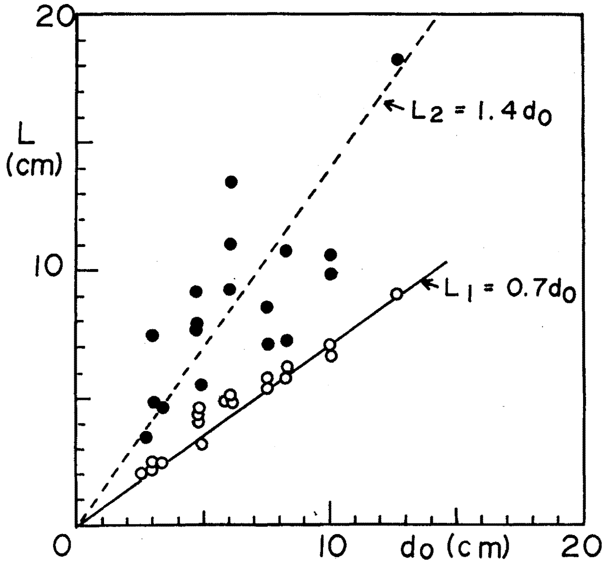

Fig. 11. Wavelengths of brick patterns observed in the present experiment.

Acknowledgments

The author wishes to express his sincere thanks to Prof. T. Tsubaki, Dr. H. Honji and Dr. M. Hirano for valuable suggestions and discussions. He also wishes to thank Y. Shiraishi and N. Matsunaga for technical help.

References

1) Bagnold, R. A. : *Motion of Waves in Shallow Water : Interaction between Waves and Sand Bottoms*, **Proc. R. Soc. London A-187**, 1946, 1-18.
2) Inman, D. L. : *Wave-Generated Ripples in Nearshore Sands*, U. S. **Army Beach Erosion Board TM 100,** 1957.
3) Yalin, M. S. & Russel, R. C. H. : *Similarity in Sediment Transport Due to Waves*, **Proc. 8th Coastal Engng. Conf. Mexico City,** 1962, 151-167.
4) Kennedy, J. F. & Falcon, N. N. : *Wave-Generated Sediment Ripples*, **M. I. T. Hydrodynamic Lab. Rept.** 86, 1965.
5) Horikawa, K. & Watanabe, A. : *A Study on Sand Movement Due to Wave Action*, **Coastal Engng. in Japan 10,** 1967, 39-57.
6) Carstens, M. R., Neilsen, F. M. & Altinbilek, H. D. : *Bed Forms Generated in the Laboratory under an Oscillatory Fow*, **U. S. Army Coastal Engng. Res. Center TM 28,** 1969.
7) Dingler, J. R. & Inman, D. L. : *Wave-Formed Ripples in Nearshore Sands*, **Proc. 15th Coastal Engng. Conf. Hawaii,** 1976, 2109-2126.
8) Lofquist, K. E. B. : *Sand Ripple Growth in an Oscillatory-Flow Tunnel*, **U. S. Army Csoatal Engng. Res. Center TP 78-5,** 1978.
9) Miller, M. C. & Komar, P. D. : *Oscillation Sand Ripples Generated by Laboratory Apparatus*, **J. Sedimentary Petrology 50,** 1980, 173-182.
10) Miller, M. C. & Komar, P. D. : *A Field Investigation of the Relationship between Oscillation Ripple Spacing and the Near-Bottom Water Orbital Motions*, **J. Sedimentary Petrology 50,** 1980, 183-191.
11) Kaneko, A. & Honji, H. : *Double Structures of Steady Streaming in the Oscillatory Viscous Flow over a Wavy Wall*, **J. Fluid Mech. 93,** 1979, 727-736.
12) Honji, H., Kaneko, A. & Matsunaga, N. : *Flows above Oscillatory Ripples*, **Sedimentology 27,** 1980, 225-229.
13) Kaneko, A. : *Oscillation Sand Ripples in Viscous Fluids*, **Proc. Japan Soc. Civ. Engrs.** 307, 1981, to be published.
14) Sleath, J. F. A. : *On Rolling-Grain Ripples*, **J. Hydraulic Res.** 14, 1976, 69-81.
15) Komar, P. D. & Miller, M. C. : *The Initiation of Oscillatory Ripple Marks and the Development of Plane-Bed at High Shear Stresses under Waves*, **J. Sedimentary Petrology 45,** 1975, 697-703.
16) Kaneko, A. & Honji, H. : *Initiation of Ripple Marks under Oscillating Water*, **Sedimentology 26,** 1979, 101-113.
17) Honji, H. : *Streaked Streaming around an Oscillating Circular Cylinder*, **J. Fluid Mech.,** to be submitted.
18) Matsunaga, N. & Honji, H. : *Streaked Streaming and 'Brick Pattern' Streaming*, **Rep. Res. Inst. Appl. Mech. 88,** 1980, to be published.
19) Yalin, M. S. : *Geometrical Properties of Sand Waves*, **Proc. Am. Soc. Civ. Engrs. 90, HY-5,** 1964, 105-119.

(Recieved June 30, 1980)